Site-dependent vibrational coupling of CO adsorbates on well-defined step and terrace sites of monocrystalline platinum: Mixed-isotope studies at Pt(335) and Pt(111) in the aqueous electrochemical environment

Chung S. Kim, Wade J. Tornquist,[a] and Carol Korzeniewski[b]
Department of Chemistry, University of Michigan, Ann Arbor, Michigan 48109

(Received 10 May 1994; accepted 11 August 1994)

Infrared spectroscopy is applied to probe qualitative structural features of the adlayers formed by CO at step sites and on terrace planes of Pt(335){Pt(S)-[4(111)×(100)]} in the aqueous electrochemical environment. The C–O stretching vibrational features are reported for adlayers formed from $^{12}CO/^{13}CO$ isotopic mixtures over a wide range of CO surface coverages. At saturation, the predominant spectral features are associated with the vibrational modes of terrace-CO in terminal (atop) coordination environments. The position of the ^{12}CO and ^{13}CO spectral features and their relative intensity are examined for several $^{12}CO/^{13}CO$ fractions, and they are shown to display the characteristics of a strongly coupled system. In comparison with corresponding mixed isotope spectra for CO at Pt(111) electrodes, intermolecular coupling for terrace-CO on the (111) surface planes of Pt(335) is observed to be significantly stronger, reflecting the higher CO surface coverages on the edge sites and the terrace sites of the Pt(335) surface plane. At low coverages, spectral features associated with edge-CO are discerned, and the intermolecular coupling for atop CO is weaker than for corresponding coverages of CO at Pt(111). The weak coupling at low coverages is attributed to the exclusive CO occupation at the step edges, which confines the intermolecular coupling to one dimension, in the direction along the step edges. For all coverages, values are determined for the dynamic dipole–dipole coupling parameter ($\Delta\nu_d$) and the chemical (static–dipole) shift parameter ($\Delta\nu_s$). Values for $\Delta\nu_s$ are generally small at all coverages. Values for $\Delta\nu_d$ are small (<8 cm^{-1}) at low coverages, where CO forms one-dimensional structures along the step edges, and they increase to large values (~ 42 cm^{-1}) at coverages that coincide with the growth of two-dimensional structures on the terrace planes. The majority of measurements were made for the Pt(335) electrode at potentials in the classical double-layer region, although dipole coupling parameters are also reported for Pt(335)/CO at potentials in the hydrogen adsorption region, where $\Delta\nu_d$ approaches zero at low coverages.

I. INTRODUCTION

In studies of mechanistic surface chemistry, it is of basic interest to define the influence of defect structures on the overall rate and specificity of chemical transformations.[1–4] In addressing questions in this area, an important strategy has been to probe fundamental aspects of adsorption and reactivity at stable high index surface planes of monocrystalline metals. These materials have structurally well-defined step and kink structures, which serve as models for the surface defect sites found on materials that are commonly used in practical catalytic applications.

Several recent papers in this area have reported on site-dependent phenomena at Pt(335) {Pt-(S)-[4(111)×(100)]}.[3–16] This surface was originally used to support infrared spectroscopic studies of carbon monoxide (CO) adsorption at defect sites on small platinum catalyst particles,[13,14] and it has since become a model substrate for vibrational studies of site-dependent adsorption processes. The earliest experiments defined conditions for observing independent vibrational spectral features for molecules on Pt(335) step edges (edge-CO) and for molecules on Pt(335) terrace planes (terrace-CO).[12,13] Subsequent investigations have used this knowledge to explore aspects of site-dependent interfacial phenomena, such as electric field inhomogeneities at surface defects,[5,8,10,11,16] site-specific CO oxidation,[6,9] and molecular interactions at stepped monocrystalline electrode surfaces.[3,4]

A notable property of Pt(335)/CO is that the CO occupancy at step and terrace sites is determined by the surface coverage, as CO preferentially binds sites on the step edge, and begins to occupy terrace sites only after the edge sites fill.[3–6,8–13] At low coverages, vibrational features for edge-CO are observed, whereas at intermediate and high coverages, vibrational features for terrace-CO appear. An important characteristic of this system is that the relative intensity of the edge- and terrace-CO infrared spectral features for corresponding coordination environments (i.e., terminal, twofold bridging, etc.) do not provide a quantitative measure of the relative CO population at these sites. For species in terminal coordination environments, the intensity of the lower energy edge-CO feature diminishes with increasing CO surface coverage, as the terrace sites fill. These intensity alterations occur on account of strong intermolecular interactions between edge- and terrace-CO molecules, and several vibrational spectroscopic studies of Pt(335)/CO have observed the effect.[3–13]

Our work on Pt(335)/CO has focused on probing site-

[a]Department of Chemistry, Eastern Michigan University, Ypsilant, MI 48197.
[b]Corresponding author.

 0021-9606/94/101(10)/9113/9/$6.00

dependent interfacial processes under aqueous electrochemical conditions.[3,4] It is part of an effort in electrochemical surface science that aims to derive structural information on molecular adlayers at single crystal metal electrodes through comparative studies on corresponding surface/adsorbate systems in ultrahigh vacuum (UHV).[17,18] Infrared spectroscopy has played a major role in supporting work in this area (see Refs. 17–20 for reviews). While the majority of these infrared spectroscopic studies have examined CO adsorption at the low index surface planes of platinum and rhodium, similar experiments using well-ordered high index surface planes of single crystal electrodes have recently appeared,[3,4,21–23] and work with Pt(335)/CO is the first of these to observe specific site-dependent phenomena.[3,4] Initial studies identified conditions for observing edge- and terrace-CO infrared spectral features in aqueous electrochemical environments by adapting approaches used in the earliest UHV studies of Pt(335)/CO.[3] Then, by working under conditions where independent spectral features for edge- and terrace-CO could be observed, it was shown that edge-CO molecules undergo potential induced structural alterations that correlate with hydrogen adsorption/desorption processes.[4]

The present work examines qualitative structural characteristics of CO adlayers at Pt(335) electrodes through experiments that probe the vibrational properties of $^{12}CO/^{13}CO$ isotopic mixtures. This approach has been most commonly used in UHV studies of molecular adsorption at single crystal metals (cf. Refs. 24–26), and it was recently extended to probe structural aspects of CO adlayers at Pt(111) electrodes.[27] Isotopic mixture experiments provide a measure of the extent of adsorbate–adsorbate intermolecular coupling, which is related to gross structural features of the adlayer.[24–34] In the Pt(335)/CO isotopic mixture experiments reported here, two approaches were used to derive adlayer structural information. The first was only applied at saturation coverages, where the vibrational spectral features under study were associated with CO on the terrace planes. Under these conditions, spectra were recorded over a wide range of $^{12}CO/^{13}CO$ fractions, and the extent of intermolecular coupling was assessed qualitatively, from the relative intensity of the ^{12}CO and ^{13}CO vibrational features.[25,28,29] By comparing relative intensity data for Pt(335)/CO and Pt(111)/CO, the effect of regular step structures on the adlayer formed on the short (111) terrace planes was evaluated. The second approach involved using established procedures for determining the dynamical dipole–dipole coupling parameter ($\Delta\nu_d$) and the static dipole (or chemical) shift parameter ($\Delta\nu_s$) from the ^{12}CO and ^{13}CO vibrational mode frequencies measured over a wide range of CO surface coverages and $^{12}CO/^{13}CO$ fractions.[24–34] Dipole coupling parameters were measured for edge-CO and for terrace-CO and used to evaluate gross adlayer structural features at step and terrace sites.

In these experiments, the measured dipole–dipole coupling parameters were small when only the edge sites were occupied, but the dynamical component increased to large values with increasing terrace-CO occupancy. The coverage dependence of $\Delta\nu_d$ is consistent with a model of the CO adlayer in which the intermolecular coupling is confined to one dimension at low coverages, in the direction along the step edge, but extends to two dimensions as the terrace sites fill. At coverages near saturation, the extent of intermolecular coupling for CO on the (111) terrace planes of Pt(335) was greater than for CO on Pt(111), reflecting the higher CO surface coverages on the edge and terrace sites of Pt(335).

II. EXPERIMENT

The equipment and experimental methods used to obtain infrared spectra of CO on monocrystalline metal electrodes have been described previously.[3] The Pt(335) single crystal disk (7 mm diam by 2 mm thick) (Aremco) and the Pt(111) single crystal disk (9 mm diam by 3 mm thick) (Materials Preparation Facility at Cornell University) were oriented to within $\pm 1°$. The orientation was verified in our laboratory by x-ray back diffraction. The flame annealing method, as described in Ref. 4 was used to clean and order the platinum surface planes prior to spectroscopic experiments.

Spectral measurements were made with the crystal disk working electrode in a three electrode electrochemical cell[3] that was constructed from Kel–F and fitted with a trapezoidal calcium fluoride window (Solon Technologies, Solon, OH). CO adlayers were formed by dosing the electrode at a fixed potential from electrolyte solutions that contained dissolved CO at dilute ($\sim 4\times10^{-5}$ M) levels.[3,27]

Dosing solutions were prepared from stock 0.1 M $HClO_4$ electrolyte solutions that contained $^{12}CO/^{13}CO$ mixtures at a total CO concentration of about 10^{-3} M. The stock dosing solutions were prepared from natural carbon monoxide gas (Matheson, 99.5% purity) and $^{13}C^{16}O$ (Cambridge Isotope, 99.95% purity, with less than 0.1% $^{13}C^{18}O$). The bulb containing $^{13}C^{16}O$ was fitted with a vacuum stopcock before use. Stock $^{12}CO/^{13}CO$ electrolyte solutions were prepared in a 45 ml mixing flask that contained two ports, each fitted with a vacuum stopcock. Just before solutions were needed, the mixing flask was connected to the reagent bulb via a 10 ml, three-port expansion chamber, which was connected to a pumping system though one port via a vacuum stopcock. Both the mixing flask and expansion chamber were evacuated and then sealed, after which the stopcock on the ^{13}CO reagent bulb was opened, allowing $^{13}C^{16}O$ to fill the expansion chamber. Once the expansion chamber was filled with $^{13}C^{16}O$, the stopcock on the reagent bulb was closed to prevent loss of reagent in subsequent steps. $^{13}C^{16}O$ from the expansion chamber was then leaked into the mixing flask by opening the connecting vacuum stopcock, leaving the final $^{13}C^{16}O$ pressure in the mixing flask at a small fraction of 1 atm. Then, about 35 ml of fresh 0.1 M $HClO_4$ electrolyte solution, previously argon purged and ^{12}CO saturated, was fed into the mixing flask through the second port. The mixing flask was then disconnected from the system, and shaken for about 30 min, which gave a $HClO_4$ electrolyte solution that was about 10^{-3} M CO, with a ^{12}CO composition of about 10%. Solutions with a higher percentage of ^{12}CO were prepared by displacing a portion of $^{13}C^{16}O$ in the mixing flask with ^{12}CO, just prior to admitting the electrolyte solution. Dosing solutions were prepared from aliquots of the stock solution by withdrawing a small portion from the mixing flask and diluting it in an appropriate volume of fresh $HClO_4$ electrolyte held in the electrochemical cell.

The spectroelectrochemical cell contained a platinum ring counter electrode and a saturated calomel electrode (SCE) reference. CO dosing was performed with the electrode potential held fixed at −0.2 V. In all experiments, the cell potential was controlled by using a Pine AFRDE4 potentiostat (Pine Instruments, Grove City, PA) and potentials are reported with reference to the saturated calomel electrode (SCE).

Infrared spectra were obtained using a Digilab FTS-40 Fourier transform infrared spectrometer equipped with a liquid nitrogen cooled narrow band MCT detector. Interferograms were recorded at a resolution of 4 cm^{-1}, and a triangular apodization function was used in the Fourier transformation. In recording the reported spectra, the electrode was held at the indicated potential while 1024 interferograms were coadded, signal averaged, and then Fourier transformed to give a (sample) single beam spectrum. A reference single beam spectrum was recorded at the end of each experiment by stepping the potential to +0.6 V (vs SCE), where adsorbed CO is removed from the surface through its oxidation to CO_2. Absorbance spectra were then computed from the ratio of the sample and reference single beam spectra. The CO surface coverage was determined from the integrated absorbance of the solution $^{13}CO_2$ and $^{12}CO_2$ peaks at 2275 and 2343 cm^{-1}, respectively.[3,18,27] Coverages are reported as a fraction of the saturation values (θ/θ_{max}).

Electrolyte solutions were prepared from perchloric acid (Aldrich, redistilled, 99.999% purity) using distilled water that was further purified by using a Barnstead Nanopure II cartridge system followed by oxidation processing under ultraviolet irradiation (Barnstead organic pure).

III. RESULTS

Initial experiments examined saturated CO adlayers, and the spectral features were recorded for a wide range of $^{12}CO/^{13}CO$ fractions. In subsequent experiments, the spectral features of these isotopic mixtures were recorded for submonolayer coverages. In the majority of experiments, spectra were collected at 0.1 V (vs SCE), in the classical double-layer region, where the electrode is free of oxides, and the only coadsorbed species are water and supporting electrolyte anions. The double-layer region is typically the most appropriate to examine when making comparisons with UHV studies of CO adsorption. Some results of spectral measurements made with the electrode at −0.2 V, in the classical hydrogen adsorption region, are also presented. These latter experiments probe the influence of hydrogen coadsorption on the CO spectral features and are of general interest in studies of interfacial electrochemistry.

A. Mixed isotope experiments on saturated CO adlayers

Initial experiments were conducted on saturated CO adlayers, where strong terrace-CO spectral features are observed. Spectra were recorded for several $^{12}CO/^{13}CO$ isotope ratios, spanning a wide range of composition. Selected spectra from these experiments are shown in Fig. 1. The C–O stretching vibrational features for atop CO are displayed, and the features show the intensity alterations that are characteristic of intermolecular coupling.[24–26] The $^{12}CO/^{13}CO$ isotopic doublet is only discernible for fractional ^{12}CO compositions below about 30%. Above 30%, only the higher energy feature appears, which is associated with in-phase adlayer vibrational motion that is predominantly $^{12}C–O$ stretching in character (for a discussion on adlayer vibrational mode assignments, see Refs. 25, 28, and 29). The feature associated with coupled vibrational motion of ^{13}CO species, present at 2015–2007 cm^{-1}, only displays significant intensity when the fraction of ^{13}CO in the adlayer is greater than about 80%.

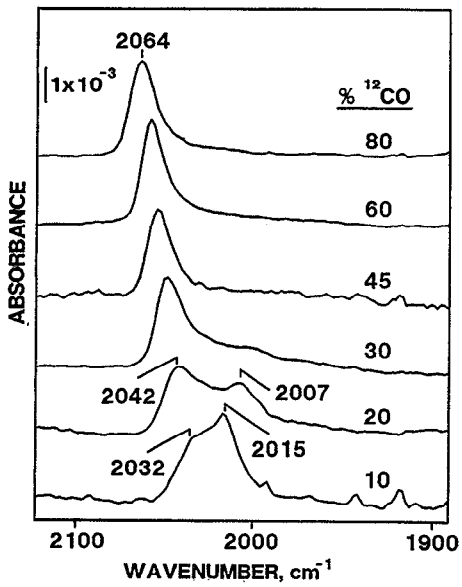

FIG. 1. Spectra showing the C–O stretching vibrational features for a saturated CO adlayer at Pt(335) for different $^{12}CO/^{13}CO$ fractions, expressed as the percentage of ^{12}CO in the adlayer, as indicated. The Pt(335) electrode was maintained at a potential of 0.1 V (vs SCE) in an aqueous 0.1 M $HClO_4$ electrolyte solution.

Figure 2(a) summarizes the frequency shifts for a large number of mixed isotope experiments. In all cases, the CO adlayer was saturated and the Pt(335) surface plane was maintained at fixed potential under aqueous electrochemical conditions. The higher energy branch shows the upshift in the ^{12}CO band frequency that occurs as the ^{12}CO percent composition increases, and the lower energy branch shows the corresponding decrease in frequency associated with the ^{13}CO feature. Since the $^{13}C–O$ stretching vibrational feature cannot be discerned for ^{12}CO compositions greater than about 30% (Fig. 1), the lower energy branch on the plot in Fig. 2(a) does not extend beyond this point. Figure 2(b) shows the data set for Pt(335) from Fig. 2(a) plotted together with results from corresponding mixed isotope experiments conducted using a Pt(111) electrode. This plot allows the degree of CO intermolecular coupling on Pt(335) and Pt(111) to be compared, which is useful for assessing how step sites perturb the structure of the CO adlayer that forms on (111) surface planes. In this plot, the lower energy branch for Pt(111)/CO extends out to about 80% ^{12}CO percent composition, considerably higher than the corresponding branch for Pt(335)/CO. This behavior indicates that the Pt(111)/^{13}CO features survive out to high ^{12}CO fractional compositions, in

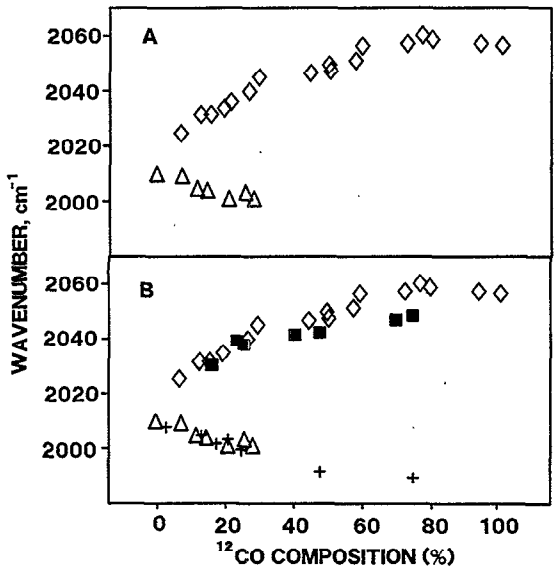

FIG. 2. Plots showing the peak frequency of the C–O stretching vibrational features for saturated CO adlayers at Pt(335) (A and B) and Pt(111) (B) for different $^{12}CO/^{13}CO$ fractions, expressed as the percentage of ^{12}CO in the adlayer. The upper branch of each plot records the frequency response of the ^{12}CO spectral features, while the lower branch records the response of the ^{13}CO spectral features. Symbols are for modes of ^{12}CO at Pt(335) (open diamonds), ^{12}CO at Pt(111) (from Ref. 27 for dosed adlayers) (filled squares), ^{13}CO at Pt(335) (open triangles), and ^{13}CO at Pt(111) (from Ref. 27, for dosed adlayers) (crosses). The Pt(335) and Pt(111) electrodes were maintained at a potential of 0.1 V (vs SCE) in an aqueous 0.1 M $HClO_4$ electrolyte solution.

contrast to $Pt(335)/^{13}CO$. These intensity effects appear in the representative mixed isotope spectra shown in Fig. 3. Panel 3(a) compares the $^{12}CO/^{13}CO$ isotopic doublet for intermediate isotopic compositions. On Pt(335), the ^{13}CO feature is reduced to a weak shoulder when the ^{13}CO composition reaches 70% (or equivalently, when the ^{12}CO composition reaches 30%), but on Pt(111), a ^{13}CO spectral band is present at lower dilutions, appearing at 2006 cm^{-1} at

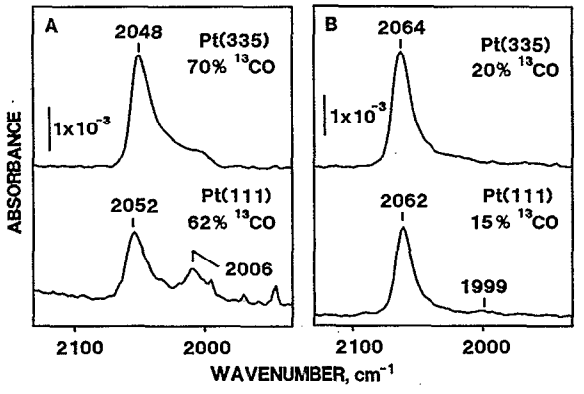

FIG. 3. A comparison of the C–O stretching spectral features for saturated adlayers of CO at Pt(335) (top) and Pt(111) (bottom) for intermediate (A) and small (B) $^{12}CO/^{13}CO$ fractions, expressed as the ^{13}CO percent composition. The Pt(335) and Pt(111) electrodes are maintained at a potential of 0.1 V (vs SCE) in an aqueous 0.1 M $HClO_4$ electrolyte solution.

62% ^{13}CO composition (38% ^{12}CO composition). Panel 3(b) displays the isotopic doublet for small ^{13}CO fractions. The ^{12}CO feature at 2064–2062 cm^{-1} is dominant, but the weak ^{13}CO feature at Pt(111) indicates that the dilution limit for this isotope has just been reached. In these saturation coverage experiments, the intensity of the ^{13}CO spectral features for specific ^{13}CO (or ^{12}CO) fractions suggests that the intermolecular coupling interactions for CO on Pt(111) are weaker than for terrace-CO on Pt(335).

B. Mixed isotope experiments on adlayers formed at subsaturation coverages: A separation of the "chemical" and "dynamical" components of the frequency shifts

Mixed isotope experiments that probe CO spectral features at fixed total CO surface coverage, as in the saturation coverage experiments discussed above, maintain the chemical environment within the adlayer as constant—the mass changes only disrupt the extent to which individual oscillators are coupled through dynamical dipole–dipole interactions.[24–26,28–34] By varying the CO surface coverage, alterations in the internal chemical bonding of adsorbed species can occur through coverage-dependent changes in the surface charge density.[24–26] These chemical effects perturb the adlayer principal and interaction force constants. Mixed isotope experiments conducted under specified coverage conditions allow a separation of the chemical (or static) and dynamical contributions to the adlayer vibrational frequency shifts (i.e., $\Delta\nu_s$ and $\Delta\nu_d$, respectively).[24–26,29–32,35–37]

For Pt(335)/CO, traditional procedures were used to determine $\Delta\nu_d$ and $\Delta\nu_s$ from coverage-dependent isotopic mixture experiments.[24–26,31,32] The dynamical component of the frequency shift was assessed for a given CO surface coverage $[\Delta\nu_d(\theta)]$ as the difference between the vibrational frequency measured at 100% ^{12}CO composition $[\nu_{CO}(\theta)]$ and the corresponding ^{12}CO dilution limit frequency $[\nu_{dl}(\theta)]$. Dilution limit frequencies were determined from plots of vibrational frequency vs ^{12}CO percent composition by extrapolating the ^{12}CO branch to zero ^{12}CO percent composition. In this limit, the ^{12}CO isotope is vibrationally decoupled from the adlayer, yet the chemical bonding interactions for the fully coupled system, at 100% composition, are maintained.[24–26] For saturation coverages, extrapolating the ^{12}CO branch in the plot shown in Fig. 2(a) gives a ^{12}CO filution limit value of 2026 cm^{-1}. Deducing ν_{CO} from this plot at 100% ^{12}CO composition allows the determination of $\Delta\nu_d$ (θ=saturation) as: 2064−2026 cm^{-1}=38 cm^{-1}.

Figure 4 shows segments of mixed isotope plots, with extrapolations out to the dilution limit frequencies, for representative surface coverages below saturation. For example, ν_{dl} is 2014, 2017, and 2025 cm^{-1} for θ/θ_{max}=0.3, 0.7, and 0.9, respectively. The ^{12}CO dilution limit frequencies increase with increasing CO surface coverage, in agreement with the trends observed for Pt(111)/CO in the electrochemical environment (see Ref. 27). It is of interest to note that, in UHV, ^{12}CO dilution limit frequencies for Pt(111)/CO follow a different coverage-dependent trend.[31,32] The difference is attributable to the platinum surface potential, which is con-

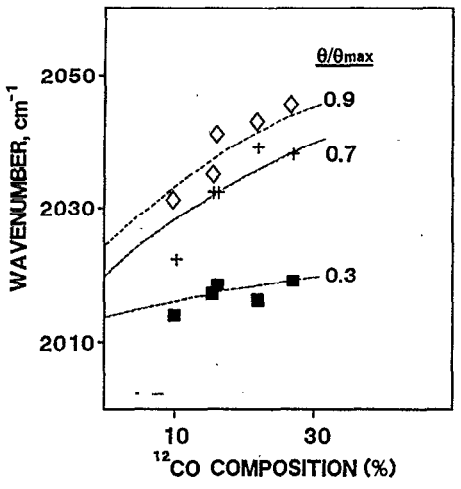

FIG. 4. The peak frequency of the ^{12}C–O stretching vibrational features are plotted against the $^{12}CO/^{13}CO$ fraction, expressed as the ^{12}CO percent composition, for different CO surface coverages. The CO surface coverages, relative to saturation (i.e., θ/θ_{max}) are as follows: 0.3 (filled squares), 0.7 (crosses), and 0.9 (open diamonds). The dashed lines indicate extrapolations to the singleton frequencies (ν_0). Data were obtained with the Pt(335) electrode maintained at a potential of 0.1 V (vs SCE) in an aqueous 0.1 M $HClO_4$ electrolyte solution.

siderably more negative in the electrochemical environment than in UHV. This issue is addressed further in Sec. IV.

Values for $\Delta\nu_d$ measured over a wide range of CO surface coverages are shown in Fig. 5. Data for two electrode

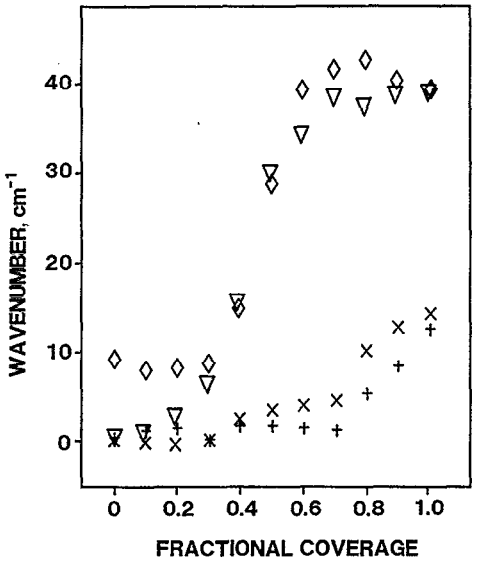

FIG. 5. Plot showing the coverage induced frequency shifts in the ^{12}C–O stretching vibrational features due to dynamic dipole–dipole coupling ($\Delta\nu_d$) and to static dipole–dipole (or chemical) interactions ($\Delta\nu_s$) as a function of the CO surface coverage at Pt(335). Data were obtained with the Pt(335) electrode maintained at constant potential (vs SCE) in an aqueous 0.1 M $HClO_4$ electrolyte solution. Symbols are for $\Delta\nu_d$ at 0.1 V (open diamonds), $\Delta\nu_d$ at −0.2 V (open triangles), $\Delta\nu_s$ at 0.1 V (exes), and $\Delta\nu_s$ at −0.2 V (crosses).

potentials (−0.2 and +0.1 V) are displayed, and overall, the coverage-dependent trends are similar for both. At low coverages, $\Delta\nu_d$ is small, which indicates that the vibrational coupling is weak under these conditions. When the fractional CO surface coverage reaches about 40%, $\Delta\nu_d$ shows a steep increase, reaching a value of about 38 cm^{-1} at 65%, after which it remains nearly constant out to saturation coverages. It is notable that the coverage dependence of $\Delta\nu_d$ displayed in Fig. 5 tracks the major coverage-dependent adlayer structural transitions that have been observed for this system.[3–6,8–13] For example, $\Delta\nu_d$ is small at low coverages, where exclusive edge-site adsorption occurs, but begins to increase as terrace sites become occupied. As discussed in detail below, the coverage dependence of $\Delta\nu_d$ shown in Fig. 5 likely reflects a transition in the vibrational coupling interactions from one to two dimensions, as the adlayer changes from exclusively edge site occupancy at low coverages to edge-terrace occupancy at intermediate and high coverages.

Figure 5 also displays values for $\Delta\nu_s$, which relate vibrational frequency perturbations to coverage-dependent changes in the surface–adsorbate chemical bonding and static dipole–dipole interactions.[24] $\Delta\nu_s$ values were computed by taking the difference between the dilution limit frequency for the surface coverage under study and the vibrational frequency of the isotope in the limit of zero *total* surface coverage [the singleton frequency for the isotope (ν_0)].[24] For the Pt(335) system, the vibrational frequency of ^{12}CO in the limit of zero coverage is about 2012 and 2004 cm^{-1} at +0.1 and −0.2 V, respectively.[3] However, these values are the edge-CO singleton frequencies, and ν_0 for terrace-CO must be determined in another way. In their UHV studies of Pt(335)/CO, Leibsle and co-workers[12] estimated the terrace-CO singleton frequency to be 9 cm^{-1} higher than the edge-CO value. We presume that they arrived at this value of 9 cm^{-1} from a plot of the atop CO band position versus CO surface coverage, by extrapolating the terrace-CO segment to zero coverage (see Ref. 12, Fig. 2). Using a similar procedure with our earlier coverage-dependent data for Pt(335)/CO (Ref. 3, Fig. 5) gives a terrace-CO singleton frequency that is about 2–4 cm^{-1} higher than the edge-CO singleton value. We also estimated the terrace-CO singleton value using the dilution limit frequency measured in the low coverage limit for terrace-CO (at $\theta/\theta_{max}=0.3$).[27,31,32,35] This latter approach gives a terrace-CO singleton frequency that is about 2 cm^{-1} higher than the edge-CO singleton value. Therefore, at high and intermediate CO surface coverages, values for $\Delta\nu_s$ were calculated using the ν_0 values 2014 and 2004 cm^{-1} for measurements at +0.1 and −0.2 V, respectively.

At low and intermediate coverages, the chemical component of the shift is small for Pt(335)/CO, and it is comparable to values measured for Pt(111)/CO under electrochemical conditions.[27] However, at high coverages, $\Delta\nu_s$ for Pt(335)/CO increases somewhat, while for Pt(111)/CO, $\Delta\nu_s$ remains small out to saturation coverages. As expected, the increase in $\Delta\nu_s$ for high CO coverages at Pt(335) parallels the coverage-dependent increase in the dilution limit values (see Fig. 4). The connection between the coverage-dependent values of $\Delta\nu_s$ measured for Pt(335)/CO and Pt(111)/CO un-

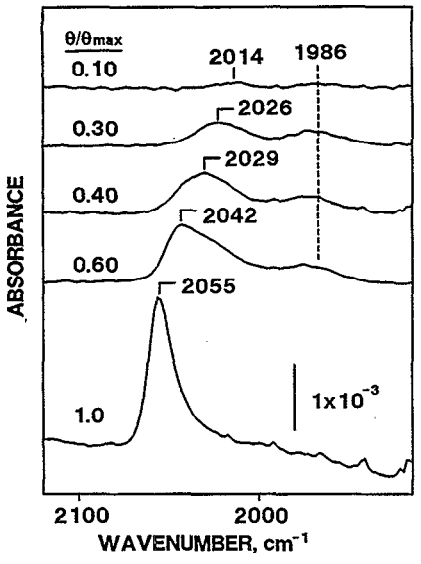

FIG. 6. The C–O stretching vibrational features for Pt(335)/CO at various surface coverages, under conditions where the ^{12}CO:^{13}CO isotopic ratio in the adlayer is 1:1. The indicated surface coverages are expressed as the fraction of saturation (i.e., θ/θ_{max}). In all experiments, the Pt(335) electrode was maintained at a potential of 0.1 V (vs SCE) in an aqueous 0.1 M $HClO_4$ electrolyte solution.

der electrochemical conditions is addressed further in Sec. IV, along with a comparison with the values for ν_{dl} and $\Delta\nu_s$ measured for Pt(111)/CO in UHV.

Computing the values in Fig. 5 required knowledge of the spectral features over a wide range of surface coverages and isotope compositions. A sample of spectra, obtained for a ^{12}CO:^{13}CO isotopic ratio of 1:1 are shown in Fig. 6.

IV. DISCUSSION

A. Saturation coverage experiments

Mixed isotope studies on saturated CO adlayers at Pt(335) electrodes are interesting in comparison with the corresponding measurements made for CO at Pt(111) electrodes (Figs. 2 and 3). Since, at high CO coverages, the vibrational features displayed by Pt(335)/CO are characteristic of CO on (111) terrace planes, comparisons with Pt(111)/CO allow assessments to be made of the adlayer structural changes that occur when the steps disrupt the long range order of the (111) terrace plane. Of value for assessing gross adlayer structural features, is knowledge of the relative intensity of the ^{12}CO and ^{13}CO spectral features for particular ^{12}CO percent compositions. These intensity data provide a qualitative measure of the strength of the intermolecular coupling interactions, which is a function of the overall density of the adlayer.[24–26,28,31–33,38]

The physical basis for these intensity alterations has been described in several reports (cf. Refs. 24–26,28,39). A useful approach has been to consider a simple model system of coupled harmonic oscillators and deduce the relative intensities of the spectral bands from the displacement eigenvectors in combination with the surface dipole-selection rule (cf. Refs. 25 and 39). This basic analysis illustrates how the relative intensities of the spectral bands depend upon the intermolecular interactions that constrain the vibrational motion of individual oscillators and induce the collective motion that is characteristic of the adlayer vibrational normal modes. For $^{12}CO/^{13}CO$ isotopic mixtures, the disparity in the intensity of corresponding $^{12}C–O$ and $^{13}C–O$ stretching vibrational features becomes greater as the strength of the intermolecular coupling interactions increase. For highly coupled systems, the intensity of features associated with the coupled vibrational motion of ^{13}CO species diminishes in comparison to the corresponding ^{12}CO vibrational features.

For the experimental systems under study, when the adlayer ^{12}CO percent composition is less than 75%, the $^{13}CO/^{12}CO$ intensity ratio for corresponding atop features is always greater at Pt(111) than at Pt(335) (see Figs. 1–3). These intensity ratios indicate that the vibrational coupling between CO molecules on Pt(335) terrace planes is stronger than it is for CO molecules on Pt(111), and this finding suggests that these high coverage CO adlayers are denser when the long range order of the Pt(111) surface plane is disrupted by the presence of steps. This suggestion is supported by CO surface coverage measurements for Pt(335) in UHV.[8] Luo and co-workers measured a saturation coverage value of $\theta=0.63$ for Pt(335)/CO using adlayers that were dosed at 100 K and subsequently annealed at 280 K. This value is larger than the Pt(111)/CO saturation coverage, where low temperature dosing gives a coverage of $\theta=0.5$ after subsequent annealing at ambient temperatures[40,41] and a coverage of $\theta=0.58$ after annealing at 260 K.[42] Furthermore, at saturation Luo and co-workers observed full occupancy of Pt(335) edge sites, with one atop CO per edge platinum atom, and they observed half-occupancy of Pt(335) terrace sites, with atop and bridging CO in a 2:1 ratio on the terrace.[8] This adlayer structure is expected to display strong atop CO intermolecular coupling, on account of the high population of atop CO on the terrace planes and the large number of edge-CO/terrace-CO interactions. For a similar adlayer structure formed at Pt(335) in the electrochemical environment, it is expected that the $^{13}CO/^{12}CO$ intensity transfer characteristics would be comparable to the effects observed in the present experiments. Therefore, in comparison to Pt(111)/CO, the stronger intermolecular coupling for Pt(335)/CO at saturation likely reflects the higher CO surface coverage at both the edge and the terrace sites of Pt(335). The relative importance of these two contributions will become better defined through experiments that probe these terrace-CO coupling interactions at a series of structurally related Pt(S)-[n(111)×(100)] surface planes.

B. Coverage-dependent experiments

1. Dipole–dipole coupling interactions

Mixed isotope experiments performed at coverages below saturation are useful for identifying features of adlayer structures that form along the steps, and they also provide a measure of coverage-dependent alterations in adsorbate chemical bonding. The coverage dependent changes in $\Delta\nu_d$ and $\Delta\nu_s$ shown in Fig. 5 summarize the important chemical

and physical properties of the adlayer at sites along the steps and on the terrace planes. It was mentioned earlier that the small value for $\Delta\nu_d$ at low coverages is characteristic of weak coupling interactions encountered when the molecules form one-dimensional structures along the step edges, whereas the increase in $\Delta\nu_d$ at higher coverages coincides with the formation of two-dimensional structures on the terrace planes. To derive additional information on the gross adlayer structural features, it is useful to compare results for Pt(335)/CO with corresponding experiments on Pt(111)/CO in both the electrochemical and UHV environments. To achieve this comparison, it is most convenient to calculate a quantity called the dipole shift value, $\delta(\theta)$,[31,32] which has been used in previous studies on Pt(111)/CO.[27,31,32] The dipole shift value is defined as the difference between the square of the measured adlayer vibrational frequency at a specified coverage and the square of the singleton value for that coverage $[\delta(\theta)=\nu^2(\theta)-\nu_0^2(\theta)]$. This quantity is similar to $\Delta\nu_d$, but it is used because it bears a simple, direct relationship to the interaction force constants.[31,32]

In their original work, Olsen and Masel computed values of $\delta(\theta)$ for various model CO adlayer structures on Pt(111) by using relationships that treat the intermolecular interactions by simple dipole–dipole coupling theories. They showed how the dipole shift values change in proportion to the number and density of neighboring adsorbates, and they used this information to assess the extent of CO island formation on Pt(111) in the UHV environment. Later, when Chang and Weaver studied Pt(111)/CO in the electrochemical environment,[27] they evaluated dipole shift values to support their qualitative models of the adlayer structures that form in the presence of contacting liquids. Olsen and Masel's computational study showed that plots of $\delta(\theta)$ vs θ are linear and display y-intercept values near zero, when the adlayers form as uniformly dispersed structures, but that these plots display nonlinearities and/or large y-intercept values, when the adlayers form as an array of discrete clusters. The former, nonclustering, behavior was observed in ambient temperature studies of Pt(111)/CO in UHV, whereas the response was more characteristic of island formation when the system was in contact with the aqueous electrochemical environment.

In Fig. 7, the dipole shift values obtained in the present study for Pt(335)/CO are plotted together with the corresponding values for Pt(111)/CO from earlier experiments. For Pt(111)/CO, Fig. 7(b) compares the frequency response for the system under UHV and electrochemical conditions. As described above, the response in UHV is essentially linear and approaches zero at low coverages, which is typical of adlayers that form uniformly dispersed structures. In the electrochemical environment, Pt(111)/CO data display a nonlinear response, especially at low coverages, where the upward curve in the plot is characteristic of island formation. Also, in the high coverage region of this plot, the Pt(111)/CO dipole shift values are larger in the electrochemical environment than in UHV, suggesting that the adlayers formed in UHV are more weakly coupled. Further support for this idea has come from recent low energy electron diffraction (LEED) studies, which examined CO adlayers on Pt(111)

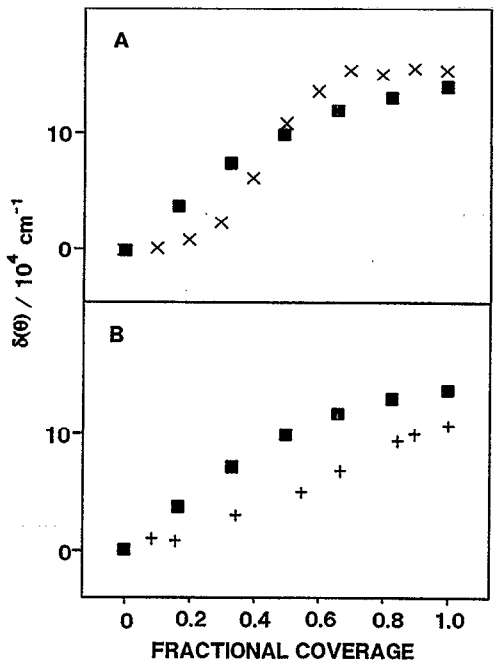

FIG. 7. Plots showing the coverage induced change in the dipole shift parameter, $\delta(\theta)$, which is computed as the difference between the square of the measured $^{12}C-O$ stretching adlayer vibrational frequency at a specified coverage and the square of the corresponding singleton value for that coverage $[\delta(\theta)=\nu^2(\theta)-\nu_0^2(\theta)]$. (A) A comparison of dipole shift values for Pt(335) (crosses) and Pt(111) (squares, from Ref. 27, for dosed adlayers) under electrochemical conditions. (B) A comparison of the frequency response for Pt(111)/CO under UHV (crosses, from Ref. 32) and electrochemical conditions (squares).

electrodes, after the electrodes were dosed with CO in the aqueous environment and then subsequently transferred into UHV.[40] At high coverages, the CO adlayer adopts the highly compressed $(\sqrt{3}\times3)$-rect structure on Pt(111) electrodes. The $(\sqrt{3}\times3)$-rect structure is denser than the $c(4\times2)$ structure that forms when Pt(111) is dosed with CO at ambient temperatures in UHV;[40] therefore, adlayers formed in the electrochemical environment are expected to be more strongly coupled than in UHV, on account of their closer proximity. An important property of the infrared technique is that it can detect these subtle differences in the adlayer structures.

Figure 7(a) shows the dipole shift values for CO adlayers formed in the aqueous electrochemical environment at Pt(111) and Pt(335). At coverages near zero, the extent of island formation is small for both systems, as indicated by the near zero y intercepts. As the CO surface coverage begins to increase, the rapid rise in the Pt(111)/CO dipole shift value indicates that CO clusters begin to form at an early stage, whereas the essentially constant dipole shift for Pt(335)/CO, out to about 30% of saturation, indicates that the extent of CO cluster formation is quite small for this system. The different responses can be linked to the step sites on Pt(335), which enhance the stability of the surface–adsorbate bond relative to Pt(111).[8,13,15] Since CO prefers to occupy sites along the step edge, at low coverages the CO molecules are spatially separated in the dimension perpendicular to the steps. Therefore, when the molecules assemble along the step

edge the intermolecular coupling is confined to one dimension, and as a consequence, the dipole-shift values are small. At coverages near saturation, the dipole-shift values for Pt(335)/CO exceed those for Pt(111)/CO, indicating that the coupling interactions are stronger on the short Pt(335) terrace planes than on the Pt(111) surface plane. This finding is in complete agreement with the saturation coverage mixed isotope measurements (Figs. 2 and 3).

2. Effect of electrode potential on $\Delta\nu_d$

In Fig. 5, the dipole–dipole coupling parameter and the chemical shift parameter are plotted for two electrode potentials. At high coverages, corresponding $\Delta\nu_d$ values measured at 0.1 and at -0.2 V are not substantially different. However, at low coverages, the $\Delta\nu_d$ values measured at -0.2 V are consistently smaller than the corresponding values measured at 0.1 V. Similar potential-dependent behavior has been reported for Pt(111)/CO, even though the specific variation of $\Delta\nu_d$ with coverage is somewhat different for the two systems.

The potential-dependent variation in $\Delta\nu_d$ likely results from at least two factors acting in combination. The first is the metal surface potential, which has a profound influence on the structure of CO adlayers.[17,19,43–48] In particular, as the potential is made increasingly negative, a fraction of the atop CO population shifts into sites of two- and threefold bridging coordination. For Pt(335)/CO, our earlier work observed this behavior very clearly at low CO surface coverages, where strong variations in the relative intensity of the atop and bridging C–O stretching vibrational features were observed over the potential range between 0.1 and -0.2 V.[3,4] It is expected that shifting the adlayer CO site occupancy from predominantly atop at 0.1 V to bridging coordination at -0.2 V weakens the coupling between neighboring atop CO dipoles, and as a consequence, $\Delta\nu_d$ becomes smaller. The second factor to consider in explaining the potential dependence of $\Delta\nu_d$ is hydrogen coadsorption. On an otherwise clean platinum surface, hydrogen adsorption occurs readily in the presence of low to intermediate coverages of CO.[4,18,27] The hydrogen in the adlayer can weaken CO intermolecular coupling through screening effects or by disrupting CO islands, thereby reducing the dipole–dipole coupling interactions and the magnitude of $\Delta\nu_d$. The relative importance of surface potential and hydrogen coadsorption effects on the potential dependence of $\Delta\nu_d$ cannot be discerned in these experiments. Future studies that examine this system in nonaqueous solvents, where hydrogen coadsorption cannot occur, will address this issue further.

3. Coverage and potential-dependent changes in $\Delta\nu_s$

The $\Delta\nu_s$ values reflect changes in the chemical bonding and static dipole–dipole interactions that arise through coverage-dependent changes in the surface electronic properties. In the electrochemical environment, $\Delta\nu_s$ values measured for Pt(335)/CO (Fig. 5) show a close correspondence to the values reported for Pt(111)/CO,[27] except at high coverages, where $\Delta\nu_s$ takes on larger positive values at Pt(335). It is difficult to explain the disparities in the $\Delta\nu_s$ values at high coverages. One consideration is the possible error in the terrace-CO singleton frequencies; however, the steep increase in $\Delta\nu_s$ occurs over the range of θ/θ_{max} between 0.7 and 1.0, where the change in $\Delta\nu_s$ (i.e., $\Delta\Delta\nu_s$) is independent of the singleton value. Disparities in the $\Delta\nu_s$ values are more likely to be a consequence of the different adlayer structures that form at Pt(111) and Pt(335), and the higher saturation CO surface coverage at Pt(335) could be an important factor. It is also of interest to note that the increase in $\Delta\nu_s$ at $\theta/\theta_{max}=0.7$ (Fig. 5) nearly coincides with the onset of a major adlayer structural transition, observed by Luo and coworkers at $\theta/\theta_{max}=0.63$ in their UHV studies of Pt(335)/CO.[8]

Another important aspect to consider is the relationship between the chemical shift values for CO at platinum in the electrochemical and UHV environments. For Pt(111)/CO in UHV, early work by Crossley and King[29,30] determined $\Delta\nu_s$ to be essentially zero, but more recent studies by Olsen and Masel indicate that $\Delta\nu_s$ shifts increasingly negative with higher surface coverages, reaching a value of -14.4 cm^{-1} at saturation.[31,32] The latter coverage-dependent response coincides with values of $\Delta\nu_s$ measured for CO adlayers at copper, where substantial downward shifts have been reported.[35,37,49] The chemical shift values measured for Pt(111)/CO in the electrochemical environment are close to the values that Crossley and King determined in their early UHV experiments, but they differ in comparison to Olsen and Masel's more recent UHV work. Also, the negative chemical shift values that Olsen and Masel observe at high coverages in UHV run counter to the increasingly positive values observed for Pt(335)/CO in the electrochemical environment (Fig. 5).

Given the paucity of isotopic mixture experiments for $^{12}CO/^{13}CO$ on platinum, a lengthy discussion of subtle differences between the various systems is unwarranted. However, more general comments can be made, which relate the differences in surface potential for the various systems to the magnitude and sign of the chemical shift values. For example, aside from CO at platinum electrodes, the only other system to display positive chemical shift values is Pd(100)/CO in UHV, where $\Delta\nu_s$ approaches $+60$ cm^{-1} at saturation.[36] In the palladium system, the CO site occupancy is predominantly bridging,[36] as a consequence of extensive surface electron charge delocalization from the metal into the $2\pi^*$ orbitals on CO.[36] The predominantly bridging CO site occupation on Pd resembles the increased bridging coordination that occurs for CO at platinum (and rhodium)[43] electrodes as the electrode potential is made increasingly negative (i.e., Refs. 18 and 48). Therefore, these conditions that promote extensive metal $\rightarrow\pi^*$ backdonation, also give rise to positive values of $\Delta\nu_s$. This tendency is also displayed in the potential dependent changes in $\Delta\nu_s$ measured for Pt(111)/CO in the electrochemical environment, where $\Delta\nu_s$ takes on negative values at $+0.1$ V and shifts positive at -0.2 V.[27]

A final remark relates to the dilution limit frequencies, which shift higher in energy with increasing CO surface coverage in the electrochemical environment (Fig. 6 and Ref. 27), but shift to lower energy with increasing CO surface coverage in UHV.[31,32] Since $\Delta\nu_s$ is simply the difference

between ν_{dl} and the singleton frequency, the same electronic factors that influence the magnitude and sign of $\Delta\nu_s$ (discussed immediately above) are expected to be important in determining the dilution limit frequencies. Continuing studies on adlayers formed from isotopic mixtures will further define the physical and chemical factors that influence $\Delta\nu_s$ and ν_{dl}.

V. SUMMARY

$^{12}CO/^{13}CO$ isotopic mixture experiments have provided qualitative insights into the local CO adlayer structures that form at step sties and on terrace planes of Pt(335) electrodes in the aqueous electrochemical environment. The intermolecular coupling interactions were found to be weakest over a range of low coverages, where the CO occupation on Pt(335) is predominantly along the step edges. At these low coverages, the dynamical dipole–dipole coupling interactions were found to be smaller at Pt(335) than at Pt(111), presumably on account of the preferred CO occupancy at step sites, which induces the CO molecules on Pt(335) to order along the steps and to spatially separate in the direction perpendicular to the steps. At higher CO surface coverages, where CO begins to occupy terrace sites on Pt(335), an increase was observed in the dynamical dipole–dipole coupling parameter, coincident with the onset of two-dimensional adlayer growth on the terrace planes. At coverages near saturation, the static and dynamical dipole–dipole coupling parameters were found to be larger for Pt(335)/CO than for Pt(111)/CO, reflecting the higher CO surface coverages on the edge sites and the terrace sites of Pt(335). Finally, at low coverages, the dynamical dipole–dipole coupling parameter for Pt(335)/CO became smaller as the electrode potential was lowered. The potential-dependent variation in the dynamical dipole–dipole coupling interactions was attributed to a combination of potential induced adlayer restructuring and hydrogen coadsorption.

ACKNOWLEDGMENTS

We thank Professor Mark Severson for helpful discussions of dipole-coupling theories. W.J.T. gratefully acknowledges support from the Eastern Michigan University sabbatical leave program. This work was supported by grants from General Electric and the Office of Naval Research.

[1] G. A. Somorjai, *Chemistry in Two Dimensions: Surfaces* (Cornell U.P., Ithaca, NY, 1981).
[2] M. A. Henderson, A. Szabo, and J. T. Yates, Jr., J. Chem. Phys. **91**, 7245 (1989).
[3] C. S. Kim, W. J. Tornquist, and C. Korzeniewski, J. Phys. Chem. **97**, 6484 (1993).
[4] C. S. Kim, C. Korzeniewski, and W. J. Tornquist, J. Chem. Phys. **100**, 628 (1994).
[5] J. S. Luo, R. G. Tobin, D. K. Lambert, G. B. Fisher, and C. L. DiMaggio, J. Chem. Phys. **99**, 1347 (1993).
[6] J. Xu and J. T. Yates, Jr., J. Chem. Phys. **99**, 725 (1993).
[7] H. J. Jansch, J. Xu, and J. T. Yates, Jr., J. Chem. Phys. **99**, 721 (1993).
[8] J. S. Luo, R. G. Tobin, D. K. Lambert, G. B. Fisher, and C. L. DiMaggio, Surf. Sci. **274**, 53 (1992).
[9] J. Xu, P. Henriksen, and J. T. Yates, Jr., J. Chem. Phys. **97**, 5250 (1992).
[10] D. K. Lambert and R. G. Tobin, Surf. Sci. **232**, 149 (1990).
[11] J.-S. Luo, R. G. Tobin, D. K. Lambert, F. T. Wagner, and T. E. Moylan, J. Electron Spectrosc. Relat. Phenom. **54/55**, 469 (1990).
[12] F. M. Leibsle, R. S. Sorbello, and R. G. Greenler, Surf. Sci. **179**, 101 (1987).
[13] B. E. Hayden, K. Kretzschmar, A. M. Bradshaw, and R. G. Greenler, Surf. Sci. **149**, 394 (1985).
[14] R. G Greenler, K. D. Burch, K. Kretzschmar, R. Klauser, A. M. Bradshaw, and B. E. Hayden, Surf. Sci. **153**, 338 (1985).
[15] R. G. Greenler, F. M. Leibsle, and R. S. Sorbello, Phys. Rev. B **32**, 8431 (1985).
[16] R. G. Greenler, J. A. Dudek, and D. E. Beck, Surf. Sci. **145**, L453 (1984).
[17] M. J. Weaver and X. Gao, Annu. Rev. Phys. Chem. **44**, 459 (1993).
[18] S. C. Chang and M. J. Weaver, J. Phys. Chem. **95**, 5391 (1991).
[19] X. Gao, S. C. Chang, X. Jiang, A. Hamelin, and M. J. Weaver, J. Vac. Sci. Technol. A **10**, 2972 (1992).
[20] C. Korzeniewski and M. W. Severson, Spectrochim. Acta (in press).
[21] S. C. Chang, A. Hamelin, and M. J. Weaver, J. Phys. Chem. **95**, 5560 (1991).
[22] S. C. Chang, A. Hamelin, and M. J. Weaver, Surf. Sci. **239**, L543 (1990).
[23] S. Watanabe, J. Inkai, and M. Ito, Surf. Sci. **293**, 1 (1993).
[24] B. E. Hayden, in *Vibrational Spectroscopy of Molecules on Surfaces*, edited by J. T. Yates, Jr., and T. E. Madey (Plenum, New York, 1987), Vol. 1, p. 267.
[25] P. Hollins and J. Pritchard, Progr. Surf. Sci. **19**, 275 (1985).
[26] R. F. Willis, A. A. Lucas, and G. D. Mahan, in *The Chemical Physics of Solid Surfaces and Heterogeneous Catalysis,* edited by D. A. King and D. P. Woodruff (Elsevier, Amsterdam, 1983), Vol. 2, p. 59.
[27] S. C. Chang and M. J. Weaver, J. Chem. Phys. **92**, 4582 (1990).
[28] R. M. Hammaker, S. A. Francis, and R. P. Eischens, Spectrochim. Acta **21**, 1295 (1965).
[29] A. Crossley and D. A. King, Surf. Sci. **68**, 528 (1977).
[30] A. Crossley and D. A. King, Surf. Sci. **95**, 131 (1980).
[31] C. W. Olsen and R. I. Masel, J. Vac. Sci. Technol. A **6**, 792 (1988).
[32] C. W. Olsen and R. I. Masel, Surf. Sci. **201**, 444 (1988).
[33] M. W. Severson, W. J. Tornquist, and J. Overend, J. Phys. Chem. **88**, 469 (1984).
[34] M. W. Severson, A. Russell, D. Campbell, and J. W. Russell, Langmuir **3**, 202 (1987).
[35] D. P. Woodruff, B. E. Hayden, K. Prince, and A. M. Bradshaw, Surf. Sci. **123**, 397 (1982).
[36] A. Ortega, F. M. Hoffman, and A. M. Bradshaw, Surf. Sci. **119**, 79 (1982).
[37] P. Hollins and J. Pritchard, Surf. Sci. **89**, 486 (1979).
[38] B. N. J. Persson and R. Ryberg, Phys. Rev. B **24**, 6954 (1981).
[39] D. K. Paul, T. P. Beebe, Jr., K. J. Uram, and J. T. Yates, Jr., J. Am. Chem. Soc. **114**, 1949 (1992).
[40] D. Zurawski, M. Wasberg, and A. Wieckowski, J. Phys. Chem. **94**, 2076 (1990).
[41] N. R. Avery, J. Chem. Phys. **74**, 4202 (1981).
[42] H. Steininger, S. Lehwald, and H. Ibach, Surf. Sci. **123**, 264 (1982).
[43] S. L. Yau, X. Gao, S. C. Chang, B. C. Schardt, and M. J. Weaver, J. Am. Chem. Soc. **113**, 6049 (1991).
[44] J. D. Roth, S.-C. Chang, and M. J. Weaver, J. Electroanal. Chem. **288**, 285 (1990).
[45] S.-C. Chang, X. Jiang, J. D. Roth, and M. J. Weaver, J. Phys. Chem. **95**, 5378 (1991).
[46] J. D. Roth and M. J. Weaver, Langmuir **8**, 1451 (1992).
[47] X. Jian and M. J. Weaver, Surf. Sci. **275**, 237 (1992).
[48] N. Kizhakevariam, X. Jiang, and M. J. Weaver, J. Chem. Phys. **100**, 6750 (1994).
[49] R. Ryberg, Surf. Sci. **114**, 627 (1982).